



Supplementary Information for

Functional modulation of PTH1R activation and signaling by RAMP2

Katarina Nemeč^{1,2}, Hannes Schihada^{2,3}, Gunnar Kleinau⁴, Ulrike Zabel², Eugene O. Grushevskiy^{1,2}, Patrick Scheerer^{4,5}, Martin J. Lohse^{1,2,6*}, Isabella Maiellaro^{2,7*}

1. Max-Delbrück-Center for Molecular Medicine in the Helmholtz Association (MDC), 13125 Berlin, Germany
2. Institute of Pharmacology and Toxicology, University of Würzburg, 97078 Würzburg, Germany
3. Section of Receptor Biology & Signalling, Dept. Physiology & Pharmacology, Karolinska Institute, S17177 Stockholm, Sweden
4. Charité - Universitätsmedizin Berlin, corporate member of Freie Universität Berlin and Humboldt-Universität zu Berlin, Institute of Medical Physics and Biophysics, Group Protein X-ray Crystallography and Signal Transduction, Charitéplatz 1, 10117 Berlin, Germany.
5. Deutsches Zentrum für Herz-Kreislauf-Forschung (DZHK), partner site Berlin, Berlin, Germany
6. ISAR Bioscience Institute, 82152 Munich, Germany
7. School of Life Sciences, Queen's Medical Centre, University of Nottingham, NG7 2UH Nottingham, UK

This PDF file includes:

Supplementary methods
Figures S1 to S14
Tables S1 to S5

Supplementary methods

Structural homology modelling of PTH1R-ligand-RAMP2-Gs complexes

To obtain three-dimensional homology models of putative arrangements between RAMP2 and PTH1R bound with the peptidic ligands PTHrP or PTH, several available structural templates were used^{16,51}. It should be noted that the native PTH ligand in complex with the PTH1R receptor and both together with a cofactor protein RAMP have not yet been structurally determined. The following aspects must be mentioned for building a complex RAMP2-PTH1R-PTH structural model.

First, the PTH1R structure determined so far in complex with long-acting PTH and Gs protein (LA-PTH, Fig.S12A-B1) provides a suitable receptor starting template for the design of complexes with both PTH and PTHrP as well as with RAMP2.

Second, an appropriate structural template for detailed RAMP2 binding to PTH1R is the CLR-CGRP-RAMP1 complex, which has also already been solved (Fig. S12 B2). This complex shows an overall and detailed binding mode of RAMP1 and provides information about the orientation of the membrane-spanning RAMP-helix and the extracellular RAMP-domain at the receptor-ligand complex. The RAMP2-adrenomedullin-receptor structure (AM1R) is also available⁵² (PDB ID: 6uun), but most of the side chains in the extracellular parts are not visible in the structure, making it less suitable for homology modeling purposes.

Third, it is further important to note that the spatial orientation of the receptor extracellular domain (receptor-ECD) in complex with the ligand relative to the transmembrane domain (TMD) of the receptor differs substantially between the two templates PTH1R-LA-PTH and RAMP-bound CLR-CGRP (or AM1R complex) structures (Fig. S12 B3). Both RAMP-binding, as well as different ligand conformations, can cause these differences. Both the PTH1R and CLR are similar in the receptor-ECD sequences and especially in their structural folding (Fig. S12A, S12B4), but the bound ligands are distinct in their secondary structures and overall arrangement to the receptor-ECD (with the ligand C-terminus) and to the transmembrane region (with the ligand N-terminus) (Fig. S12B1-B2). In the case of PTH1R, the LA-PTH ligand forms a straight helix from the ECD to the TMD at the receptor (Fig. S12B1). In contrast, the bound CGRP or adrenomedullin in the CLR or AM1R, respectively, is kinked, and the C-terminus is unfolded compared to the straight LA-PTH helix (Fig. S12B2, B4). Notably, the ECD folding of the receptor is similar when comparing the structures of apo-ECD, RAMP1-CLR, or CLR-RAMP1-CGRP complexes (Fig. S12B5), which is not indicative for global structural changes in the ECD of the receptor due to the binding of ligands or RAMPs. Due to the specific orientations of the CLR-ECD and differences in the length of extracellular loop 2 (EL2), the N-terminus of the CGRP ligand is orientated slightly diverse compared to LA-PTH in the transmembrane receptor part (Fig. S12B3, upper figure), whereby the CGRP ligand is shifted towards TM1 and TM2 of the CLR compared to the LA-PTH orientation in the PTH1R.

Fourth, analysis of amino acid contacts between RAMP2 and the CLR ECD without ligand (Fig. S13 top sequence comparison and left structure at the bottom) shows that essential amino acids in the receptor ECD contacting RAMP2 (red lines) are also present in the N-terminal extracellular PTH1R sequence (Fig. S13, third sequence), e.g., amino acids Q45 and E54 (similar to Q54 in CLR). This fact supports the possibility that the RAMP2 ECD also binds to the PTH1R ECD in a mode comparable to that observed for the CLR-ECD-RAMP1 complex. In addition, corresponding and identical receptor amino acids in the ECD, such as R162, are involved in the binding of LA-PTH to PTH1R, and CGRP to CLR, respectively (Fig. S13, middle-right structural parts at the bottom and sequences 3 and 4 at the top), which also suggests a certain level of conservation in

the ligand binding mode, despite differences in the ligand conformation. In conclusion, in the CLR-CGRP-RAMP1 complex, a separation between receptor-ECD parts involved in either ligand or in RAMP binding can be distinguished (Fig. S12B2; Fig. S13right structure), with corresponding amino acids involved in RAMP1 binding at the CLR also found in the PTH1R-ECD (Fig. S13, sequences PTH1R and CLR ECD's). From this perspective binding of the RAMP2-ECD to the PTH1R-ECD in a manner similar to that observed for the CLR-RAMP1-CGRP complex should be feasible. Based on this assumption RAMP2 was structurally mapped to the structure of the PTH1R/ligand/G protein complex in two different ways.

On one hand, the RAMP2-ECD was bound to the PTH1R-ECD similarly to the CLR-CGRP-RAMP1 complex, retaining the entire PTH1R/LA-PTH structure already determined (Fig. S1A). The CLR-ECD apo-RAMP2 complex was superimposed with the PTH1R complex and the RAMP2-ECD was inserted into the PTH1R structure. The RAMP1-helix and the adjacent extracellular linker were added into the PTH1R complex structure after superimposition of both complexes. The RAMP1 sequence was substituted by the RAMP2 sequence (Fig. S12A, top) and the linker was manually connected to the RAMP2 ECD already merged into the initial PTH1R-ligand-RAMP2 model. Further, the LA-PTH sequence was substituted by the PTH or by the PTHrP sequences (Fig. S13, ligand sequences in the middle part), resulting in two initial homology models of the PTH1R-RAMP2-Gs complex with both ligands. These rough homology models were generated with the software SYBYL-X 2.0 (Certara, NJ, US) and optimized by energy minimization with the Amber99 force field until converging at a termination gradient of 0.05 kcal/(mol*Å) under constrained backbone atoms, followed by a 2 ns molecular dynamics simulation (MD) of side chains with constraint backbone atoms, with the exception of an un-constraint RAMP2 linker region. The entire complex was then energetically minimized without any constraint.

The second complex was generated by using the CLR-CGRP-RAMP1 complex⁵¹ (PDB ID: 6e3y) as a template for arrangements between RAMP2 toward PTH1R, and the receptor ECD toward the receptor TMD. The PTH1R ECD bound with the LA-PTH C-terminus (amino acids 22-34) was separated from the entire complex¹⁶ (PDB ID: 6nbh) and oriented towards the TM domain as supposed by the CLR-CGRP-RAMP1 complex (Fig. S12B2). The entire RAMP1 was additionally inserted from this complex into the PTH1R model, and the sequence was substituted with the RAMP2 sequence (Fig. S12A). Finally, the two ligand fragments were manually connected between the extracellular C-terminus and the bound fragment (A1-R21) in the TM region. The ligand sequence was then substituted either by the PTH or the PTHrP sequences (Fig. S13, ligand sequences in the middle part), respectively. These two models were optimized by energy minimization with the Amber99 force field until converging at a termination gradient of 0.05 kcal/(mol*Å) under constrained backbone atoms, followed by a 2 ns MD with constraint backbone atoms, except for the ligand region between AA S17-V21 (Fig. S13, ligand sequences in the middle panel). The entire complexes were energetically minimized without any constraint.

Supplementary figures

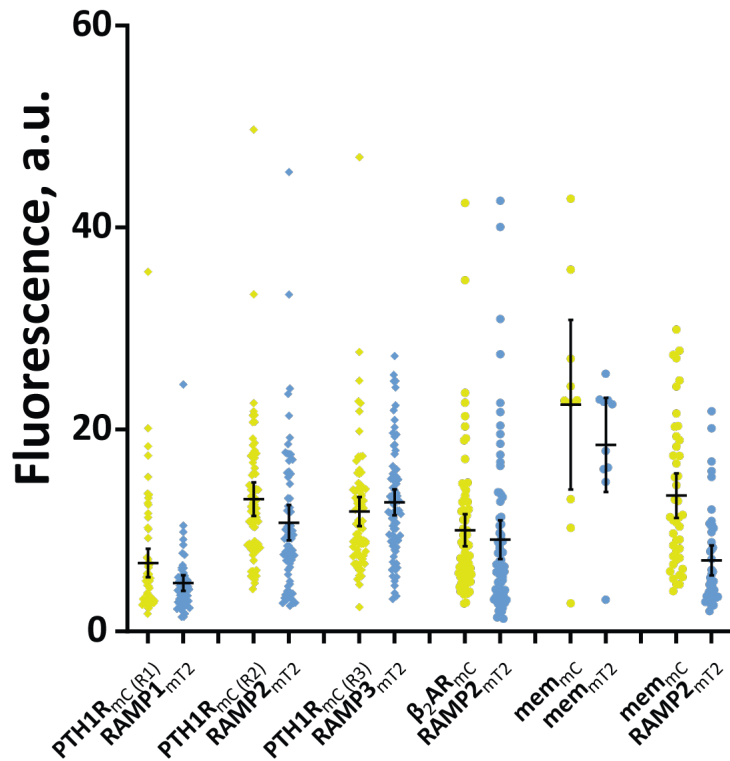


Fig. S1.

Comparison of expression levels of tagged constructs used in intermolecular FRET photobleaching experiments.

Basal fluorescence emissions of mCitrine (mC, acceptor, yellow) and mTurquoise2 (mT2, donor, cyan) before photobleaching; the experimental setting corresponds to Fig. 1. The data show individual values, means \pm SD of at least three independent experiments.

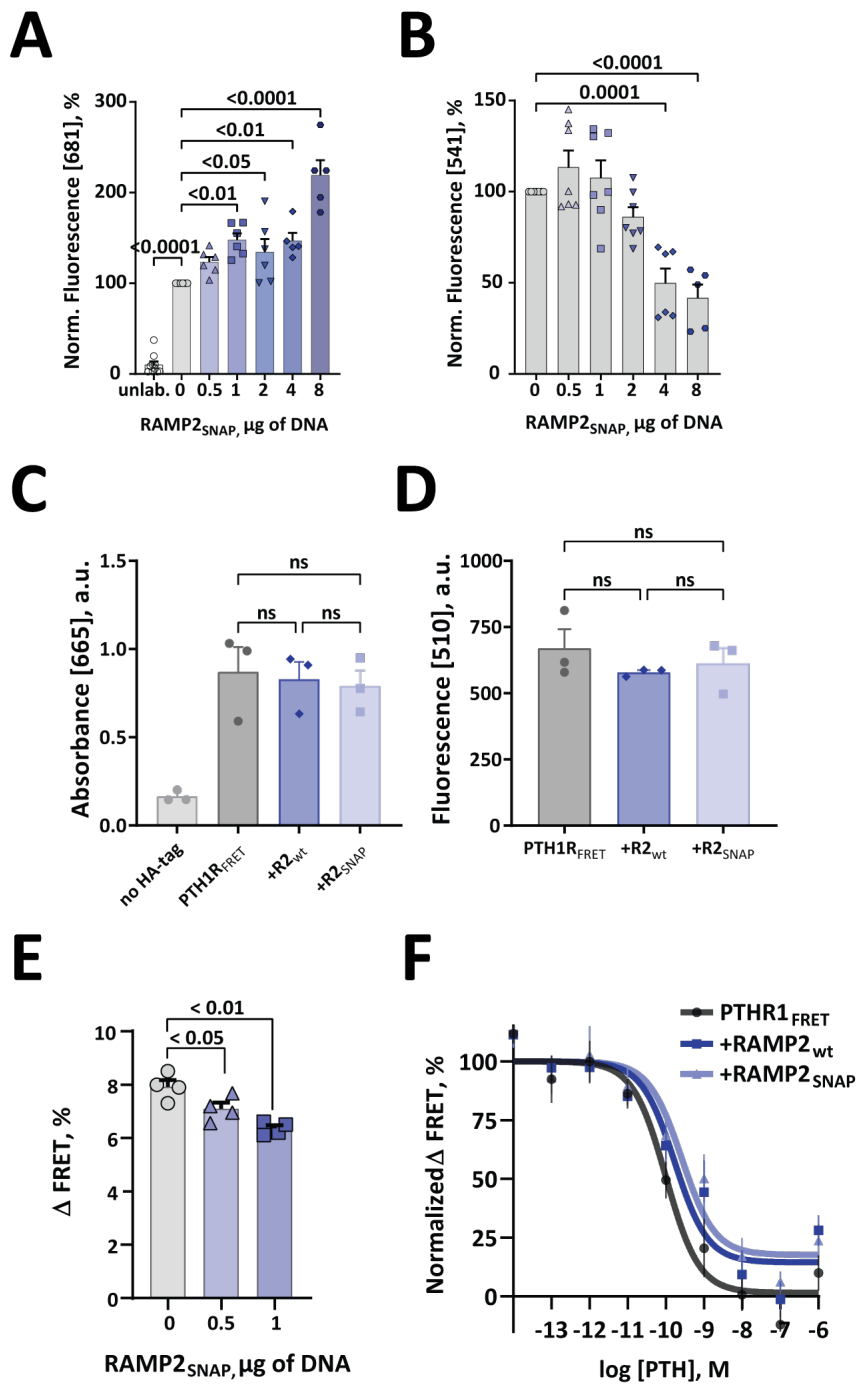


Fig. S2.

RAMP2_{SNAP} overexpression modulates PTH-induced PTH1R_{FRET} amplitude but not surface and total expression of PTH1R_{FRET} biosensor.

(A,B) HEK293 cells were transfected with the PTH1R_{FRET} biosensor plus different amounts of cDNA encoding RAMP2_{SNAP}. Emissions of SNAP-tag labeled with the 1 µM SNAP-Cell SiR-647 (A) and mCitrine (B) were collected in a plate reader. Bars represent means ± SEM; points are means of

the duplicates of individual wells from three (**A**) and five (**B**) independent experiments. Significance between the groups was tested with one-way ANOVA followed by Dunnett's multiple comparisons test; ns: $p > 0.05$.

(**C,D**) HEK293 cells transiently expressing the PTH1R_{FRET} biosensor were co-transfected with an empty control vector, RAMP2_{wt} or RAMP2_{SNAP}. (**C**) Comparison of cell surface expression levels of PTH1R_{FRET} visualized by detecting the anti-HA tag epitope fused to its N-terminus and quantified by ELISA (absorbance at 665 nm). (**D**) Comparison of total expression levels of PTH1R_{FRET} visualized by recording fluorescence of mCitrine in the same cells as in panel (**A**). The bars show means \pm SEM of three independent experiments done in quadruplicates.

(**E**) Amplitudes of FRET changes induced by 1 μ M PTH in the experiment shown in Figure 2B. Bars represent means \pm SEM from five independent experiments.

Significance between the groups in panels (**C**, **D**, **E**) was tested by one-way ANOVA, followed by Dunnett's multiple comparisons test; ns: $p > 0.05$.

(**F**) Concentration-response curves obtained in HEK293 cells stably expressing the PTH1R_{FRET} biosensor and co-transfected with RAMP2_{wt} or RAMP2_{SNAP}. Cells were stimulated with increasing concentrations of PTH. Δ FRET values are expressed as maximal change in response from the initial FRET value. The data was fitted with a three-parameter concentration-response curve fit and gave a pEC50 \pm SEM of: PTH1R_{FRET} = 9.99 ± 0.12 , +RAMP2_{wt} = 9.77 ± 0.19 , and +RAMP2_{SNAP} = 9.59 ± 0.18 . The data show means \pm SEM from three independent experiments done in quadruplicates.

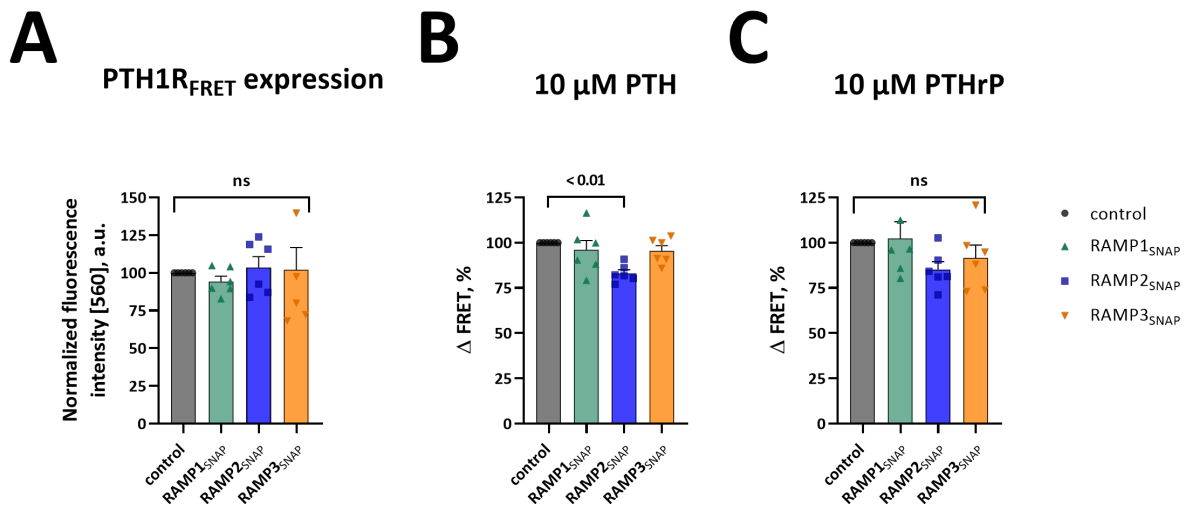


Fig. S3.

Effects of SNAP-labelled RAMP isoforms on the amplitude of PTH1R_{FRET} signals evoked by PTH and PTHrP.

HEK293 stably expressing PTH1R_{FRET} biosensor were transfected with 1 μg of cDNA encoding for one of the three RAMP_{SNAP} isoforms.

(A) Emissions of mCitrine in PTH1R_{FRET} were measured to assess the equal expression of the PTH1R_{FRET} biosensor in all experimental groups. Bars represent means ± SEM, points are means of eight replicates of individual wells from six independent experiments. Significance between the groups was tested with one-way ANOVA, followed by Dunnett's multiple comparisons test; ns: $p > 0.05$.

(B, C) Amplitudes of FRET changes in PTH1R_{FRET} induced by PTH **(B)** and PTHrP **(C)**. Bars represent means ± SEM of the FRET amplitudes from four independent experiments performed in quadruplicates. Significance between the groups was tested with one-way ANOVA, followed by Dunnett's multiple comparisons test; ns: $p > 0.05$.

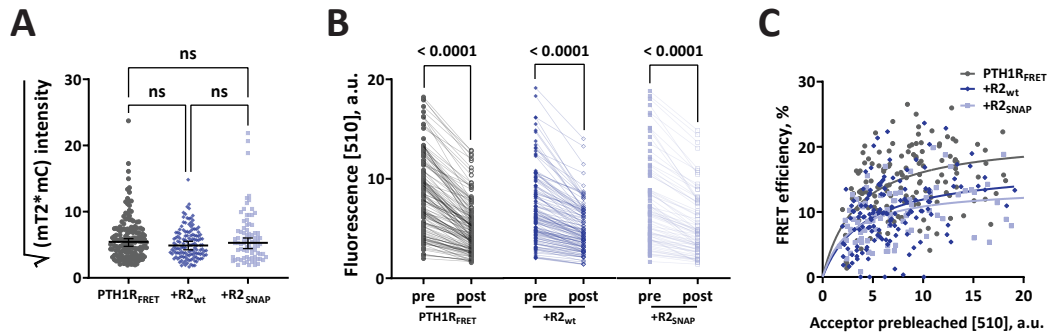


Fig. S4.

Comparison of expression levels of fluorophores and photobleaching experiments with PTH1R_{FRET} in intact HEK293 cells.

(A) Basal fluorescence emission of mCitrine (mC, acceptor) and mTurquoise2 (mT2, donor) were measured in a confocal microscope before photobleaching of HEK293 cells expressing the indicated constructs. The square root of the product of mT2 and mC normalizes for different expression levels of fluorophores to compare biosensor expression between experimental groups. The data show median emission + 95 % CI from all cells examined from four independent experiments. Each data point represents a single cell. Significance between experimental groups was determined by Kruskal-Wallis nonparametric test with Dunn's post-hoc test.

(B) Fluorescence emissions before (pre) and after (post) photobleaching shows comparable extents of photobleaching in the different experimental groups. Median photobleaching was PTH1R_{FRET} = 39.9 %, RAMP2_{wt} = 31.7 % and RAMP2_{SNAP} = 28.5 %. Significance between pre and post emission was tested with Wilcoxon paired test, ns > 0.05.

(C) FRET efficiencies of PTH1R_{FRET} in the absence or presence of RAMP2_{wt} or RAMP2_{SNAP} were calculated as described in Fig. 1. The data are plotted as a function of the emission of the acceptor before photobleaching. The curves were fitted with one site-specific binding fit. Each data point represents a single cell. Data are from the following numbers of cells obtained in four independent experiments: PTH1R_{FRET} (n = 120), +RAMP2_{wt} (n = 96), +RAMP2_{SNAP} (n = 72).

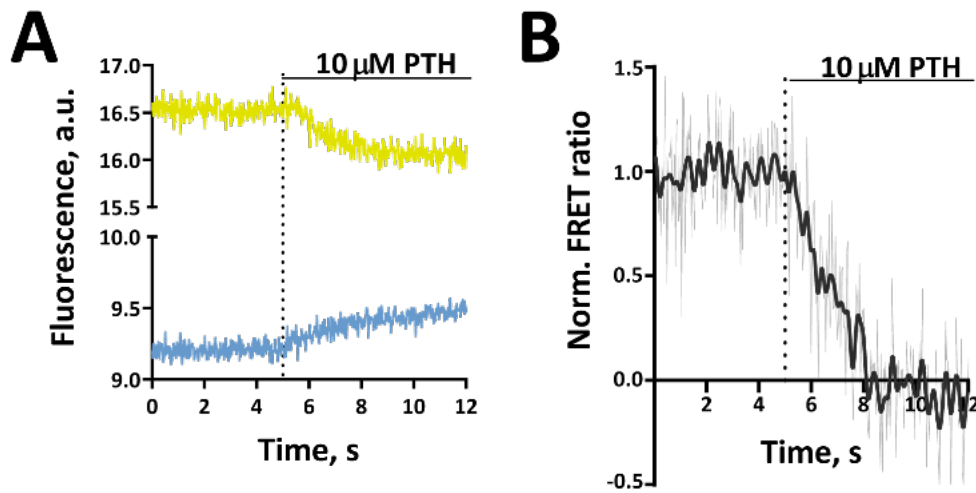


Fig. S5.

PTH-induced activation changes were recorded with the PTH1R_{FRET} biosensor.

Representative FRET traces of PTH-mediated changes in intramolecular FRET in single HEK293 cells stably expressing of PTH1R_{FRET}. Horizontal lines indicate application of 10 μM PTH with a rapid superfusion system.

(A) Traces of donor (mT2) and acceptor (mC) fluorescence.

(B) FRET ratio calculated from (A). Traces were normalized to the baseline (set to 1) and plateau after stimulation (set to 0). Shown are FRET ratio traces raw (grey) and Fourier-lowpassed (black). Traces are representative of n = 41 cells, acquired in five independent experiments.

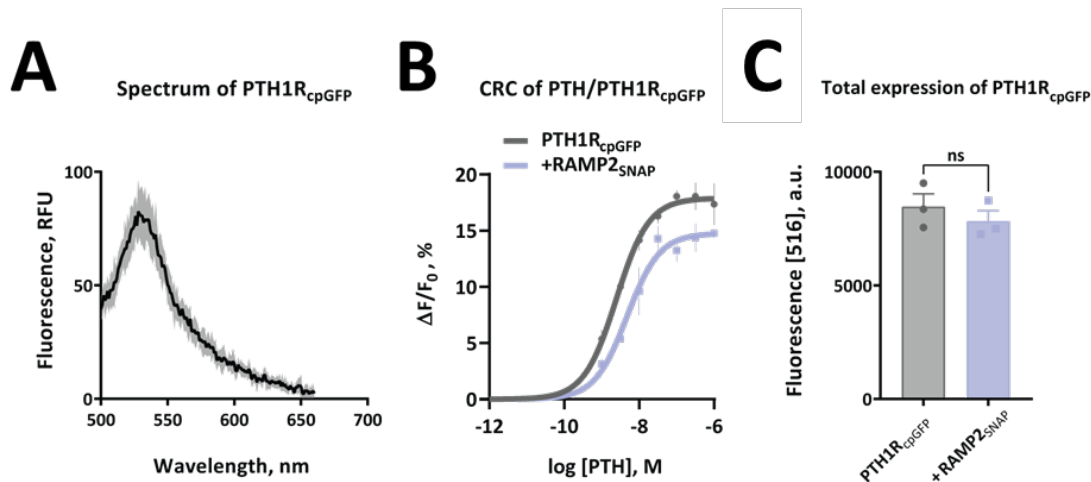


Fig. S6.

Spectral and pharmacological characterization of PTH1R_{cpGFP}.

Plate reader experiments with HEK293 cells transiently expressing the PTH1R_{cpGFP} biosensor.

(A) Fluorescence emission spectra of PTH1R_{cpGFP} upon excitation at 460 nm in the presence of 10 μ M PTH. The data are from two independent experiments done in quadruplicate and show mean \pm SEM.

(B) Concentration-response curves for stimulation with increasing concentrations of PTH. The data show mean \pm SEM of two independent experiments performed in quadruplicate. The curve was fitted with a three-parameter concentration-response curve fit, which resulted in pEC₅₀ \pm SEM of 8.61 \pm 0.07 (PTH1R_{cpGFP}) and 8.32 \pm 0.07 (+RAMP2_{SNAP}).

(C) Comparison of total expression levels for PTH1R_{cpGFP} in the absence and presence of RAMP2_{SNAP}. Shown are means \pm SEM of three independent experiments, where each individual mean was calculated from 48 wells from a single 96-well plate. A t-test was used to assess significance between the groups; ns > 0.05.

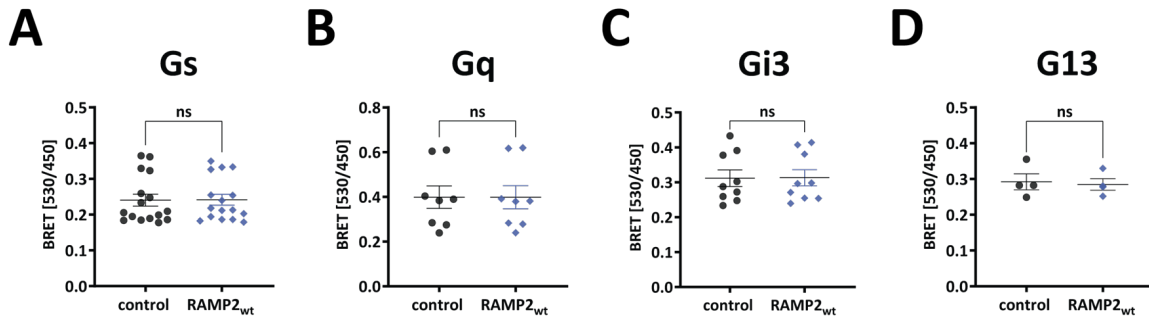


Fig. S7.

No change in basal G-protein activation evoked by RAMP2-PTH1R interaction.

HEK293 cells were transiently transfected with cDNA encoding for BRET biosensors for: Gs (**A**), Gq (**B**), Gi3 (**C**), G13 (**D**) along with PTH1R_{wt}, with or without RAMP2_{wt}. BRET signals were recorded in a plate reader without stimulation by ligand. Data are means \pm SEM of at least three independent experiments performed in duplicates or more (Gs:4, Gq:3, Gi3:4, G13:4). For each set of experiments, a t-test was used to assess a significant difference between the two groups (ns; $p > 0.05$).

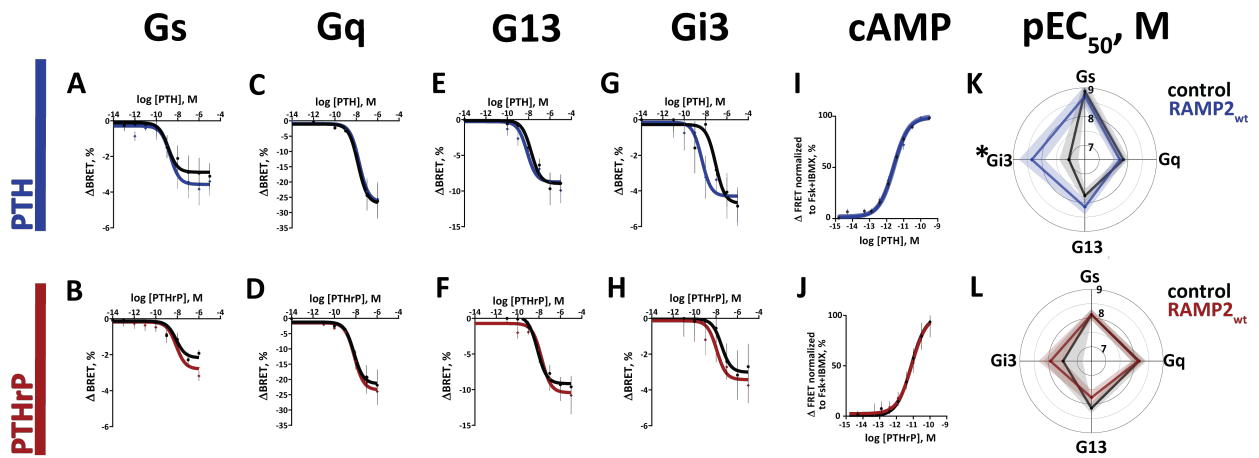


Fig. S8.

RAMP2 effects on PTH-stimulated G protein activation.

(A - H) HEK293 cells transiently transfected with cDNA encoding for BRET biosensors of Gs (A, B), Gq (C, D), G₁₃ (E, F), Gi3 (G, H) along with PTH1R_{wt}, with or without RAMP2_{wt}.

(I, L) HEK293 cells transiently transfected with cDNA encoding for the cAMP-based FRET biosensor (Epac-S^{H187}), along with PTH1R_{wt}, with or without RAMP2_{wt}.

BRET signals were recorded in a plate reader from cells stimulated with PTH (black, blue) or PTHrP (black, red). Shown are concentration-response curves, fitted with a three-parameter concentration-response curve fit. Δ BRET values were calculated in saturation and represent a maximal change in response from the initial BRET value.

Data are means \pm SEM of at least three independent experiments performed in duplicates or more. For further statistics and results see *SI Appendix*, Table S1, and S2.

(K, L) "Spider plots" showing mean \pm SEM pEC_{50} (M) values calculated from the concentration-response curves.

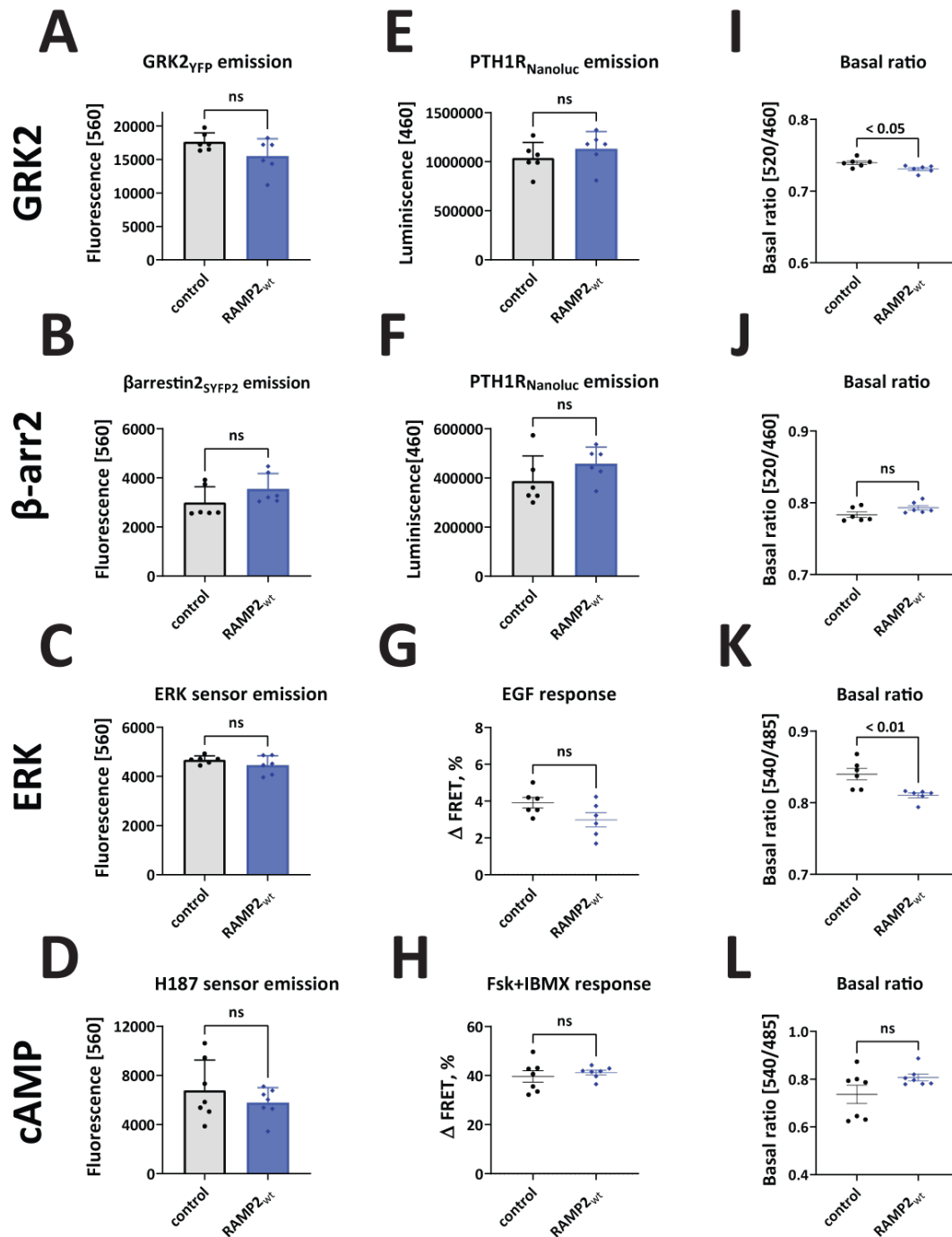


Fig. S9.

Expression controls for non-G protein functional assays.

Comparison of expression levels of constructs used in non-G protein PTH1R functional assays in the absence (grey) and presence (blue) of RAMP2_{wt}. Data were obtained in plate reader experiments with HEK293 cells transiently expressing a combination of the indicated constructs. Fluorescence emissions indicate: at 560 nm the expression level of (A) GRK2_{YFP}, (B) β-arrestin2_{mVenus}, (C) EKAR sensor and (D) cAMP biosensor Epac-S^{H187}, at 460 nm the expression level of (E - F) PTH1R_{NanoLuc}. (G) Comparison of ERK responses to 100 ng/mL Epidermal growth factor (EGF). (H) cAMP responses to 10 μM forskolin plus 100 μM IBMX. (I - L) Comparison of basal ratios before stimulation of each construct in presence of absence of RAMP2_{wt}. Shown are means ± SEM of at least three independent experiments. A t-test was used to assess significance between the groups, ns > 0.05.

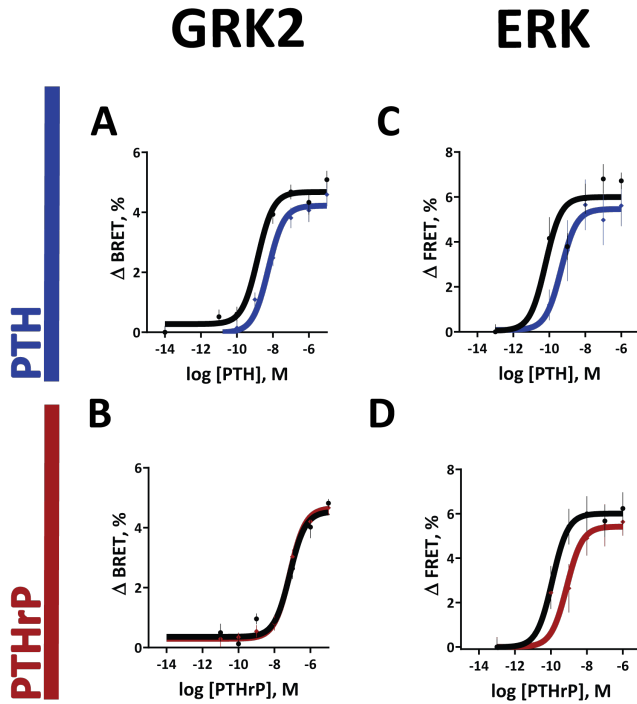


Fig. S10.

RAMP2 effects on non-G protein signalling.

(**A - D**) HEK293 cells were transiently transfected with cDNA encoding for: GRK2_{YFP} (**A, B**) along with PTH1R_{NanoLuc}, with or without RAMP2_{wt}, or with EKAR biosensor (**C, D**) along with PTH1R_{wt}, with or without RAMP2_{wt}.

BRET signals were recorded in a plate reader from cells stimulated with PTH (black, blue) or PTHrP (black, red).

Shown are time courses of agonist stimulation and corresponding concentration-response curves, fitted with a three-parameter concentration-response curve fit. Δ BRET values were calculated in saturation and represent average change in response from the initial BRET value. Data are means \pm SEM of at least three independent experiments performed in quadruplicates or more. For further statistics and results see *SI Appendix*, Table S3 and S4.

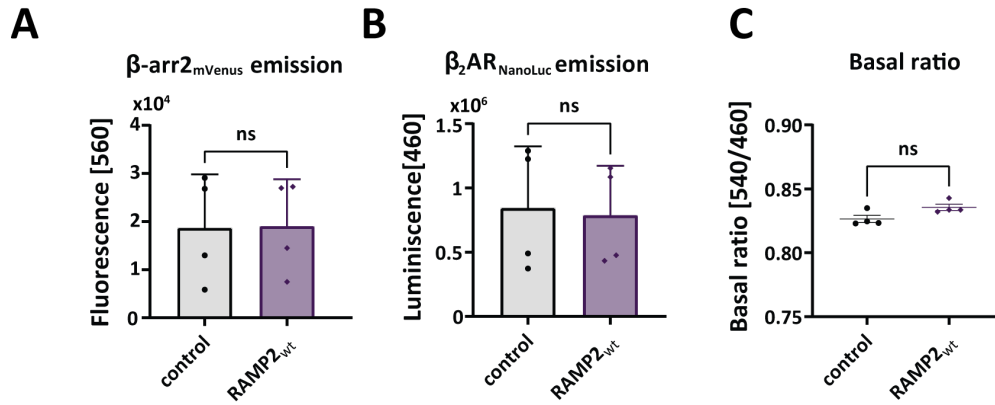


Fig. S11.

Expression controls for β -arrestin2 recruitment to β_2 AR.

(**A**, **B**) Comparison of expression levels of constructs used in the experiments for isoprenaline-induced β -arrestin2 recruitment to β_2 AR.

(**C**) Comparison of basal ratios before stimulation. All data are from four independent experiments done in quadruplicates and represent means \pm SEM where each individual mean was calculated from 48 wells in a single 96-well plate. A t-test was used to assess significance between the groups, ns > 0.05.

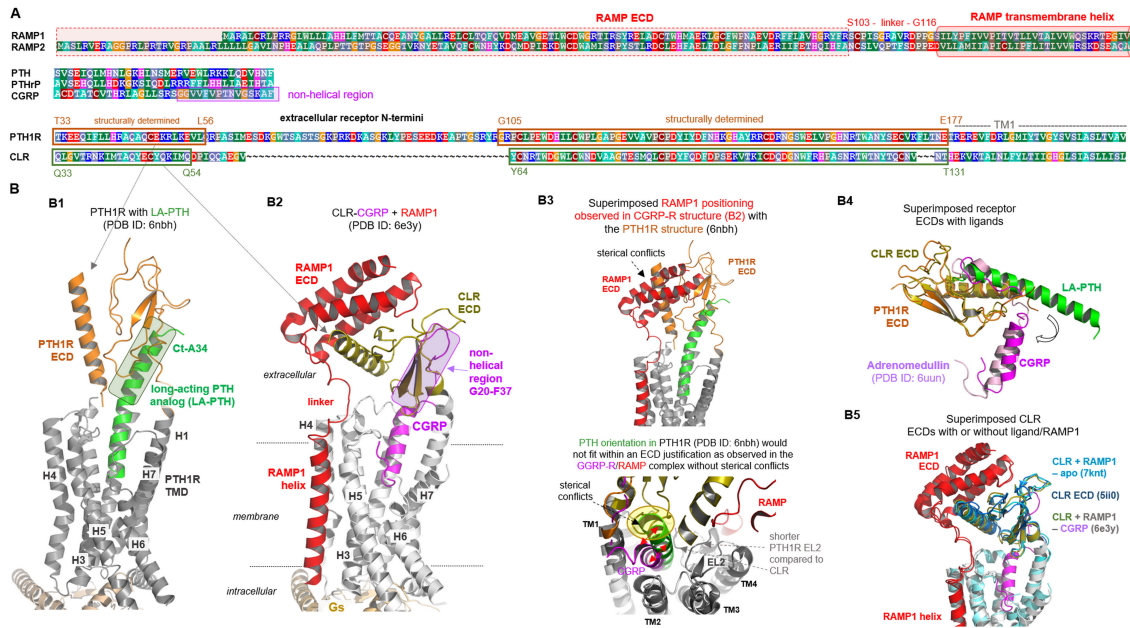


Fig. S12. Sequence and structural information used to construct PTH1R ligand-RAMP2 complexes - Part I.

(A) Sequence comparison between RAMP1 and RAMP2, ligands PTH, PTHrP, CGRP, and receptor ECDs, with highlighted dimensions in length or structural features. The alignment was visualized using the software BioEdit⁶⁸. Specific background colors reflecting chemical properties of the amino acid side chains or the type of amino acid: black-proline; blue-positively charged; cyan/green-aromatic and hydrophobic; green- hydrophobic; red-negatively charged; gray-hydrophilic; dark red-cysteines; and magenta-histidine.

(B) Structural templates for model building are visualized, including the PTH1R complex structure (B1) and the CLR-CGRP-RAMP1 complex (B2). The PDB ID's are annotated above the structures. In B3 both complexes are superimposed to highlight differences and similarities. In addition, determined receptor ECD-ligand complexes are superimposed in B4 to visualize conservation of the ECD folds, but also to show differences in the bound ligand conformations. Of note, the receptor ECDs with or without ligand and RAMP (B5) share a similar global fold, which indicates a low impact of ligand or RAMP binding on the receptor ECD core structure.

H: helix

EL: extracellular loop

IL: intracellular loop

ECD: extracellular domain

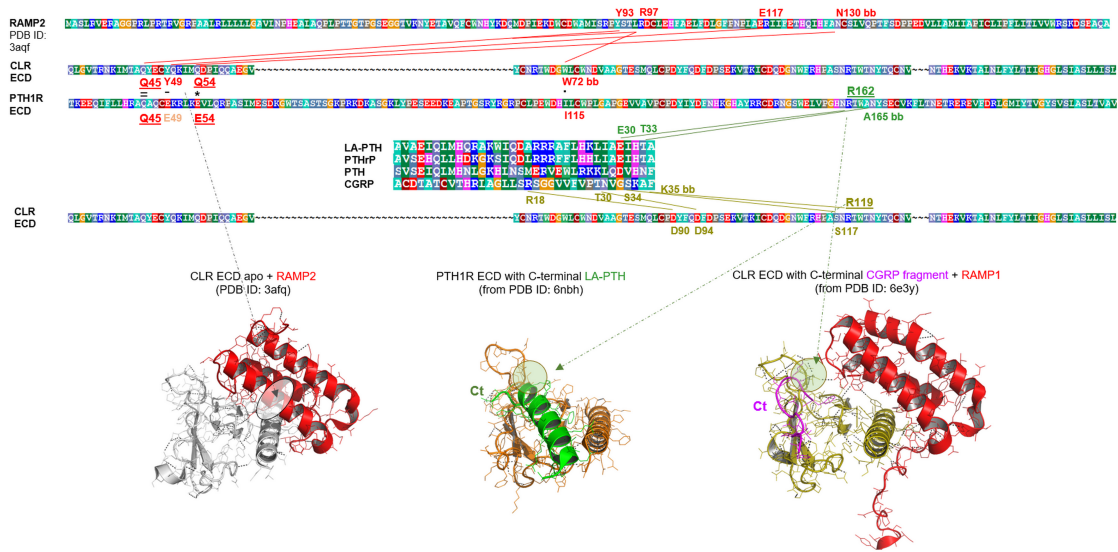


Fig. S13.

Sequence and structural information used to construct PTH1R ligand-RAMP2 complexes - Part II.

Analyses of interactions (hydrogen-bond contact distances) between RAMP2 and the CLR ECD (red lines indicating feasible interactions) reveal few essential hydrophilic contacts and similar amino acids of the CLR ECD can also be found at corresponding positions in the sequence of the PTH1R ECD (e.g. Q45 in the central contact region between receptor ECD and RAMP ECD). Moreover, ligand contacts between the ECD's of both receptors are shared by corresponding amino acids as R162, even the ligand conformation (C-terminus) is different in the bound states.

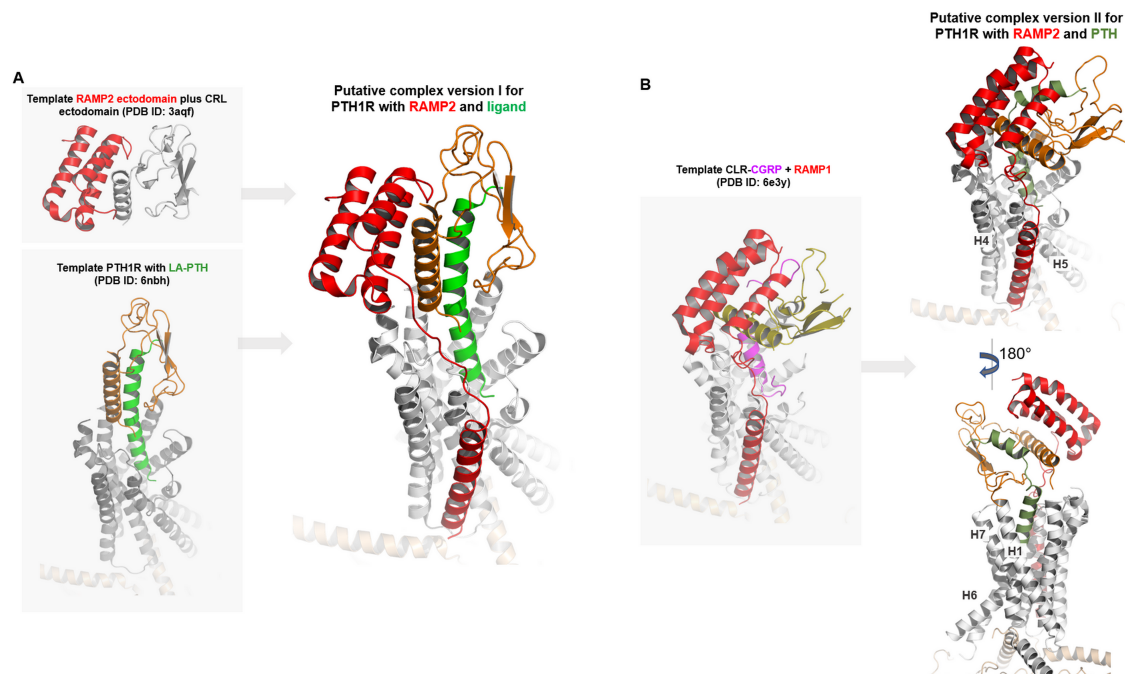


Fig. S14.

Putative structural PTH1R-ligand-RAMP2-Gs complexes.

Starting with appropriate structural templates to model putative PTH1R-RAMP-ligand complexes (PDB ID's: 6nbh, 3aqf)^{16,51,69} resulted in two versions of feasible arrangements. **(A)** In version I the RAMP2 ECD is oriented toward the PTH1R according to the already determined PTH1R-LA-PTH-Gs complex, whereby the ligand forms a regular straight helix. **(B)** Version II: Taking the already solved CLR-CGRP-RAMP1-Gs complex⁵¹ as a structural template (PDB ID: 6e3y) to adjust the complex components relative to each other, the PTH1R ECD bound with RAMP2 ECD is differently oriented toward the TMD and the ligand (e.g. PTH) must have a modified secondary structure in the central part compared to LA-PTH in the determined PTH1R complex **(A)**.

Supplementary tables

Table S1: Potency (pEC₅₀) and E_{max} values for PTH-induced G protein activation.

		PTH			<i>n</i>
		control	RAMP2 _{wt}	<i>p</i>	
G_q activation	pEC₅₀	7.84 ± 0.19	7.72 ± 0.20	ns	3
	E_{max}	26.02 ± 2.38	25.63 ± 2.35	ns	
G_s activation	pEC₅₀	8.88 ± 0.39	8.71 ± 0.36	ns	4
	E_{max}	2.78 ± 0.43	3.28 ± 0.45	ns	
G₁₃ activation	pEC₅₀	7.76 ± 0.24	8.15 ± 0.25	ns	4
	E_{max}	8.84 ± 0.90	8.47 ± 0.90	ns	
G_{i3} activation	pEC₅₀	7.06 ± 0.33	8.35 ± 0.44	< 0.05	4
	E_{max}	4.43 ± 0.68	4.16 ± 0.73	ns	
cAMP accumulation	pEC₅₀	11.57 ± 0.05	11.60 ± 0.06	ns	4
	E_{max}	100.00 ± 2.46	99.18 ± 2.86	ns	

Potency (pEC₅₀, M) and E_{max} (%) values were obtained from plate reader experiments as shown in Fig. S8. Data are means ± SEM of *n* independent experiments. Extra-sum-of-squares test was used to assess the difference between the curves, ns > 0.05.

Table S2: Potency (pEC₅₀) and E_{max} values for PTHrP-induced G protein activation.

		PTHrP		<i>p</i>	<i>n</i>
		control	RAMP2 _{wt}		
G_q activation	pEC₅₀	8.16 ± 0.25	8.13 ± 0.22	ns	3
	E_{max}	20.20 ± 2.29	21.98 ± 2.21	ns	
G_s activation	pEC₅₀	8.12 ± 0.18	8.12 ± 0.18	ns	4
	E_{max}	2.04 ± 0.27	2.62 ± 0.27	< 0.05	
G₁₃ activation	pEC₅₀	8.14 ± 0.18	7.77 ± 0.25	ns	4
	E_{max}	9.48 ± 0.74	9.72 ± 1.01	ns	
G_{i3} activation	pEC₅₀	7.49 ± 0.68	7.93 ± 0.41	ns	4
	E_{max}	2.98 ± 0.82	3.29 ± 0.58	ns	
cAMP accumulation	pEC₅₀	11.12 ± 0.14	11.08 ± 0.19	ns	4
	E_{max}	100.00 ± 8.60	97.40 ± 11.03	ns	

Potency (pEC₅₀, M) and E_{max} (%) values were obtained from plate reader experiments as shown in Fig. S8. Data are means ± SEM of *n* independent experiments. Extra-sum-of-squares test was used to assess the difference between the curves, ns > 0.05.

Table S3: Potency (pEC₅₀) and E_{max} values for PTH-induced downstream effects.

		PTH			<i>n</i>
		control	RAMP2 _{wt}	<i>p</i>	
GRK2 recruitment	pEC₅₀	8.84 ± 0.13	8.25 ± 0.14	< 0.05	3
	E_{max}	4.40 ± 0.23	4.23 ± 0.25	ns	
β-arrestin2 recruitment	pEC₅₀	9.45 ± 0.14	9.21 ± 0.12	ns	3
	E_{max}	3.66 ± 0.21	6.48 ± 0.32	< 0.05	
ERK phosphorylation	pEC₅₀	10.21 ± 0.24	9.34 ± 0.39	ns	3
	E_{max}	5.95 ± 0.76	5.39 ± 1.00	ns	

Potency (pEC₅₀, M) and E_{max} (%) values are obtained from plate reader experiments as shown in Fig. 6 and Fig. S10. Data are means ± SEM of *n* independent experiments. Extra-sum-of-squares test was used to assess the difference between the curves, ns > 0.05.

Table S4: Potency (pEC₅₀) and E_{max} values for PTHrP-induced downstream effects.

		PTHrP			
		control	RAMP2 _{wt}	<i>p</i>	<i>n</i>
GRK2 recruitment	pEC ₅₀	7.04 ± 0.12	7.23 ± 0.11	ns	3
	E _{max}	4.25 ± 0.24	4.32 ± 0.20	ns	
β-arrestin2 recruitment	pEC ₅₀	8.56 ± 0.12	8.45 ± 0.09	ns	3
	E _{max}	3.45 ± 0.16	5.85 ± 0.21	< 0.05	
ERK phosphorylation	pEC ₅₀	9.92 ± 0.40	9.12 ± 0.49	ns	3
	E _{max}	6.02 ± 0.82	5.42 ± 0.78	ns	

Potency (pEC₅₀, M) and E_{max} (%) values were obtained from plate reader experiments as shown in Fig. 6 and Fig. S10. Data are means ± SEM of n independent experiments. Extra-sum-of-squares test was used to assess the difference between the curves, ns > 0.05.

Table S5: Potency (pEC₅₀) and E_{max} values for isoprenaline-induced β -arrestin2 recruitment.

		Isoprenaline			
		control	RAMP2 _{wt}	<i>p</i>	<i>n</i>
β -arrestin2 recruitment	pEC ₅₀	7.58 \pm 0.13	7.81 \pm 0.15	ns	4
	E _{max}	2.43 \pm 0.10	2.72 \pm 0.13	ns	

Potency (pEC₅₀, M) and E_{max} (%) values were obtained from plate reader experiments as shown in Fig. S11. Data are means \pm SEM of *n* independent experiments. Extra-sum-of-squares test was used to assess the difference between the curves, ns > 0.05.